IEEE Access
Multidisciplinary ⋮ Rapid Review ⋮ Open Access Journal

Received 11 January 2023, accepted 21 January 2023, date of publication 25 January 2023, date of current version 1 February 2023.

Digital Object Identifier 10.1109/ACCESS.2023.3239798

RESEARCH ARTICLE

Development of HVDC Gas-Insulated Components for the Power Supply of Neutral Beam Injectors

FRANCESCO LUCCHINI[1,2] AND NICOLÒ MARCONATO[2,3], (Member, IEEE)
[1]CRF, University of Padova, 35122 Padua, Italy
[2]Consorzio RFX, 35127 Padua, Italy
[3]Department of Industrial Engineering, University of Padua, 35131 Padua, Italy
Corresponding author: Nicolò Marconato (nicolo.marconato@unipd.it)

ABSTRACT The development of High Voltage Direct Current Gas-Insulated components that will be employed for the power supply of Neutral Beam Injectors, requires specific numerical tools to analyze the electric field distribution, with the purpose of supporting the engineering and operational phases.The tools must comply with the nonlinearity of the material properties of solid insulators and the transport mechanisms in the dielectric gas. Despite its high Global Warming Potential, SF6 will be considered as the baseline dielectric gas for the development of HVDC gas-insulated components to be used for the Acceleration Grid Power Supply of Neutral Beam Injectors. Attention especially to the mechanisms driving to an increase of leakage current flowing in the gas, thus giving rise to possible discharge phenomena is here placed, mainly focusing on radiation and injection regimes. The described methodologies are adopted for the numerical modeling of the 500 kV DC gas-insulated components that will be used for the power supply of the Neutral Beam Injector of the Divertor Tokamak Test facility. In particular, a conceptual design of the SF6 Transmission Line and the SF6-air bushing is conceived.

INDEX TERMS Divertor tokamak test (DTT), neutral beam injector, HVDC, gas insulated transmission lines, high voltage bushing.

I. INTRODUCTION

The Neutral Beam Injector (NBI) is a key component in view of the construction of future nuclear fusion power plants, required to heat the plasma and thus reach relevant regimes. The Negative-NBI (N-NBI) accelerates a beam of negative ions, for example of Deuterium, through a series of grids at a prescribed voltage and after being neutralized, the beam enters the confinement fusion device transferring power and momentum to the plasma. The electrical power feeding the ion acceleration grids is provided by the so-called Acceleration Grid Power Supply (AGPS), while the auxiliaries required for the generation and extraction of the ions are fed by the so-called Ion Source and Extraction Power Supply (ISEPS). The whole power is delivered by a High Voltage Direct Current Gas Insulated (HVDC-GIS) Transmission Line (TL). Sulphur hexafluoride (SF_6) is usually used as insulating gas despite its high Global Warming Potential (GWP), about 23500 higher than CO_2, because of its excellent insulation properties due to the very high electron affinity. The use of alternative eco-friendly solutions is highly desirable to be adopted for the future generation of components.

Differently from HVDC-GIS apparatus employed for commercial purposes, those adopted for the AGPS have to operate under very specific conditions. First of all, for the Multi-Aperture Multi-Grid (MAMuG) configuration [1] the transmission line is not a coaxial line but is multi-conductor, since it carries also the intermediate acceleration voltages of the grids. In addition, the central conductor at the highest voltage, contains on the inside the conductors provided by ISEPS. Moreover, due to the pulsed operation of NBIs, the HVDC-GIS are not in steady state operation. In fact the typical pulse length is about 10-30 s for conventional NBIs, while for the ITER NBI, whose full-scale prototype MITICA (Megavolt ITER Injector and Concept Advancement) is being under construction at the PRIMA (Padova Research on ITER Megavolt Accelerator) test facility in Padua, Italy [2], the pulse length will be extended up to 3600 s. The NBI that will operate in the Divertor Tokamak Test facility (DTT) [3], [4], the construction of which is in the start phase in Frascati, Italy,

The associate editor coordinating the review of this manuscript and approving it for publication was Ladislau Matekovits.

has similar requirements to the one installed in JT-60SA [5] and is expected to operate with a duty cycle of 50 s every hour with a beam energy of 500 keV and 10 MW of power coupled to the plasma. In this configuration the negative Deuterium ions are accelerated by three Acceleration Grids (AGs) with -167 kV DC per stage [6], [7], [8]. Lastly, some of the HVDC-GIS components are exposed to the radiation (neutrons and γs) coming from the Tokamak, thus affecting the electrical conductivity of the insulating gas.

II. NUMERICAL MODELING OF HVDC-GIS COMPONENTS

A. ELECTRIC FIELD MODELING

Nowadays simulations tools are essential for the modeling and design of electromagnetic devices [9]. The capability of performing reliable and accurate electric field modeling is a key driver for the conceptual design of HVDC-GIS components. Historically, the transition between the initial capacitive to the stationary resistive field distribution is analyzed by means of the so-called electro-quasistatic (EQS) formulation for the electric potential φ [10]

$$\nabla \cdot \left(\varepsilon \nabla \left(\frac{\partial \varphi}{\partial t} \right) \right) + \nabla \cdot (\sigma \nabla \varphi) = 0, \tag{1}$$

where $\varepsilon = \varepsilon_r \varepsilon_0$ is the permittivity and σ the electrical conductivity of solid insulators and dielectric gas in the solution domain. Generally the electrical conductivity of solid parts depend both on temperature T and electric field E, that is $\sigma_I = \sigma_I(T, E)$. As an example, for the Alumina (Al_2O_3)-filled epoxy resin through relation [11]

$$\sigma_I(T, E) = \sigma_{I0} \exp\left(\alpha_I E + \frac{\beta_I}{T} \right), \tag{2}$$

with the parameters $\sigma_{I0} = 19.9$ S/m, $\alpha_I = 0.08$ mm/kV, $\beta_I = -W_a/k_B$ K where $W_a = 0.95$ eV and k_B the Boltzmann constant. Moreover, a non-linear conductivity can be adopted also for the surface of the solid insulator, which in the case of cast epoxy resin has the form [12]

$$\sigma_S(E_t) = \sigma_{S0} \exp(\alpha_S E_t), \tag{3}$$

where E_t is the tangential component of the electric field and the parameters can be taken as $\sigma_{S0} = 4 \cdot 10^{-18}$ S and $\alpha_S = 1.22 \cdot 10^{-6}$ m/V [12]. Surface charge density accumulating on solid-gas interfaces distorts the geometric electric field distribution, thus reducing the surface flashover voltage of solid insulator. In order to homogenize and thus reduce the field in the surface layer, different solutions were proposed. One approach consists in modifying the geometry by using the shape optimization approach [13], [14], another take advantage of particular materials such as the surface functional graded materials (SFGM) [15]. When dealing with nonlinear resistive field grading materials (FGM), for electric fields below the switching value E_1 kV/mm the material behaves as dielectric, while for stresses $E > E_1$ the material become conductive and consequently a significant increase of Joule heating takes place. The electrical conductivity of such materials can be expressed as [11]

$$\sigma_I(T, E) = \sigma_{I0} \exp\left(-\frac{W_a}{k_B T} \right) \frac{1 + \left(\frac{E}{E_1} \right)^{\gamma - 1}}{1 + \left(\frac{E}{E_2} \right)^{\gamma - 1}}, \tag{4}$$

where σ_{I0} is the specific conductivity at low electric fields and room temperature, E_2 is the saturation field and γ the slope of non-linearity. Thin layers of such compounds can be placed near the critical parts of the design with the aim of reducing the electrical stress, allowing more compact solutions [16].

The gas electric conductivity σ_G to be adopted in (1) is usually kept constant with values between 10^{-16} and 10^{-20} S/m for SF_6 [13], with a possible temperature and pressure P dependence [17]

$$\sigma_{G,SF_6}(T, P) = \sigma_{G0,SF_6} \exp\left(-\frac{W_a}{k_B T} \right) \frac{P_0}{P}, \tag{5}$$

where $\sigma_{G0,SF_6} = 1.658 \cdot 10^{-13}$ S/m, $W_a = 0.2$ eV and $P_0 = 101.325$ kPa. However, due to the presence of free ions in the insulating gas, the electrical conductivity is nor uniform neither constant and a drift-diffusion-reaction model may be adopted to analyze the electric field in a self-consistent way [12], expressed by the following governing equations

$$\frac{\partial n^+}{\partial t} = S - R n^+ n^- - \nabla \cdot (n^+ \mu^+ \mathbf{E}) + D^+ \Delta n^+ \tag{6}$$

$$\frac{\partial n^-}{\partial t} = S - R n^+ n^- + \nabla \cdot (n^- \mu^- \mathbf{E}) + D^- \Delta n^- \tag{7}$$

$$\nabla \cdot (\varepsilon \mathbf{E}) = e(n^+ - n^-), \tag{8}$$

where n^+, n^- [1/m^3] are the positive and negative ion number densities respectively and e the elementary charge. The other parameters refer to mobility (μ^+,μ^-[m^2/(V·s)]), diffusion coefficient ($D^+ = \mu^+(k_B T)/e$, $D^- = \mu^-(k_B T)/e$ [m^2/s]), recombination coefficient (R [m^3/s]) and ion-pair generation rate (S [1/(m^3 ·s)]). These parameters generally depend on experimental conditions, e.g., gas type, pressure, temperature, and electric field itself [18]. The conduction current density in the gas can be expressed as

$$\mathbf{J}_G = e\left[\mathbf{E}(\mu^+ n^+ + \mu^- n^-) - \nabla(D^+ n^+ - D^- n^-) \right] \tag{9}$$

while the surface charge density ϱ_s accumulating on the interface between solid and gas parts is written as

$$\frac{\partial \varrho_s}{\partial t} = \mathbf{n}_I \cdot (\mathbf{J}_I - \mathbf{J}_G) - \nabla \cdot (\sigma_S E_t), \tag{10}$$

where $\mathbf{n}_I$ is the normal vector to solid insulator surface and $\mathbf{J}_I$ the current density in the solid insulator domain.

For the SF_6 at the pressure of 0.5 MPa absolute in natural radiation environment, the parameters of drift-diffusion model are listed in Table 1.

B. COUPLED ELECTRO-THERMAL MODELING

The Joule heating effect caused by the current-carrying conductors is an heat source for the thermal problem, in turn,

TABLE 1. SF_6 parameters of model (6)-(7) for P=0.5 MPa for standard operational conditions.

Parameter	Value
μ^+, μ^-	$4.8{\cdot}10^{-6}$ $m^2/(V{\cdot}s)$
R	$2.27{\cdot}10^{-13}$ m^3/s
S	$2.9{\cdot}10^{7}$ $1/(m^3{\cdot}s)$

the temperature distribution may affect the electrical properties of the HVDC gas-insulated systems due to the temperature dependence of the electrical conductivities. To take into account these phenomena a coupled thermal-electrical problem have to be considered. The three main channels of heat transfer are conduction, convection and radiation, and the temperature field is mathematically described as

$$\rho C_p \left(\frac{\partial T}{\partial t} + \boldsymbol{u} \cdot \nabla T \right) = \nabla \cdot (k \nabla T) + Q, \tag{11}$$

where $\boldsymbol{u}$ is the convective velocity field, C_p [J/(kg·K)] the heat capacity, k [W/(m·K)] the thermal conductivity, ρ the density [kg/m^3] and Q [W/m^3] the heat source. For SF_6 gas the thermal conductivity generally depends on temperature, for example via a polynomial expression [17]

$$k_{SF_6}(T) = -9.51 \cdot 10^{-3} + 8.657 \cdot 10^{-5} T^2 - 3.186 \cdot 10^{-8} T^3, \tag{12}$$

while C_p is usually kept constant, moreover the gas density can be expressed with the simple ideal gas law. A summary of the typical values used in the thermal analysis of HVDC-GIS is listed in Table 2.

To account for the thermal radiation emitted by solid bodies at a certain temperature, the source term

$$Q_{rad} = \epsilon [G - n_R^2 \sigma_{SB} T^4] \tag{13}$$

has to be incorporated, where ϵ is the surface emissivity, G the irradiation [W/m^2], n_R the refractive index and σ_{SB} the Stefan-Boltzmann constant. Moreover, if the fluid motion has to be considered, the velocity of the gas in natural convection flows is retrieved by solving the Navier-Stokes equations, possibly in turbulent conditions [19]. It is worth noting that in the specific case of the TL for the NBI of DTT the thermal effects are negligible, given the low value of the transmitted current (of the order of 50 A) and the short pulse duration. We wanted to quote this paragraph for the sake of completeness, as it is considered useful for a comprehensive description of the phenomena at play and the related modelling to take it into account.

III. LEAKAGE CURRENT IN GAS AND ADDITIONAL ISSUES

Despite the dielectric gas is mostly considered as an insulator with a negligible current flowing in it, the possibility of numerically modeling such currents, however very small, is extremely important also for the experimental point of view. As a matter of fact leakage currents are always present and may be traced back to different causes, such as: external ionization fields (extremely important for HVDC-GIS used in nuclear fusion), surface roughness, water content and free

TABLE 2. Thermal parameters for SF_6 gas and epoxy solid insulator.

Parameter	Value
Cp SF_6	665.18 J/(kg·K)
Cp Epoxy	1500 J/(kg·K)
k Epoxy	0.25 W/(m·K)
ρ Epoxy	2200 kg/m^3

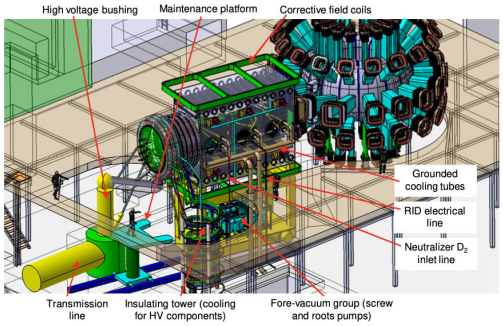

FIGURE 1. CAD overview of the DTT Tokamak hall [8]. The last part of transmission line and SF_6-air bushing is highlighted, together with the NBI and the Tokamak.

conducting metal particles. All these phenomena at the end drastically modify the dielectrical capability of the gas.

The main advantage of using the drift-diffusion model instead the EQS is in the capability of the former in accounting for the all the phenomena mentioned before. For example, the leakage current induced by external radiation is modified tuning the source parameter S in (6)-(7), while the one caused by surface roughness and small metallic tips can be modeled by introducing a Neumann condition on emitting surfaces.

A. RADIATION INDUCED CONDUCTIVITY

As mentioned earlier, the gas conductivity is due to the presence of positive and negative ion pairs, which in normal situations are generated by the natural radiation. This is taken into account by means of the source parameter S of the transport model (6)-(7).

Neutrons and gamma rays produced by fusion machine can drastically modify the electrical conductivity of SF_6 gas if the components are placed on the critical path. This effect is termed as radiation induced conductivity (RIC) whose onset led to the substitution of gas-insulated with vacuum-insulated ITER NBI beam source [20]. The vacuum insulation for the 1 MV ITER NBI is a complex task involving many technological and experimental aspects [21], [22]. For the DTT facility as shown in Fig. 1, the last part of TL and the SF_6-air bushing are currently planned to be installed inside the Tokamak hall, thus these HVDC components are subjected to radiation from the Tokamak and an estimation of the leakage current flowing in the gas is mandatory to determine the feasibility of SF_6 insulation.

Differently from the ITER NBI, whose ion source is located in vacuum, for the reason that will be clarified in the following, the design of the NBI for DTT has characteristics similar to that of the JT-60 experiment and foresees an

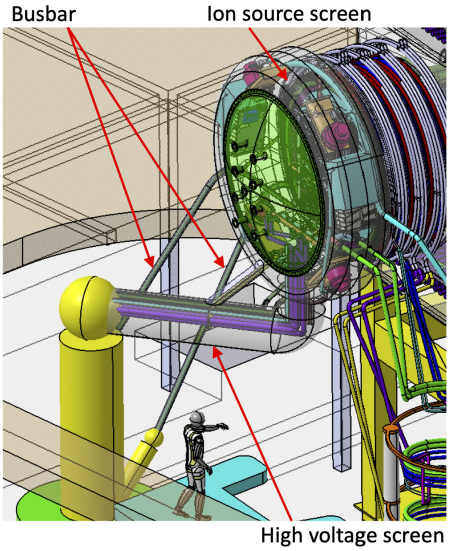

FIGURE 2. Detail of bus-bar connection of SF_6-air bushing (schematic representation) with the air-insulated beam source.

air-insulated beam source, which simplifies the design phase and increases its reliability and maintenance [8]. Therefore, the electrical connection between the TL and the acceleration grids is performed through bus-bars connected to the SF_6-air high voltage bushing, as illustrated in Fig. III-A. The major drawback of this solution is the fulfillment of stringent criteria concerning the maximum allowable electric field in air as will be explained in Sec. V-D. Similarly to ITER NBI but differently from the JT-60 solution, the DTT NBI will use a radio frequency ion source [23]. Under the irradiation field ϕ [Gy/s], the leakage current flowing in the gas for the plate-parallel geometry can be determined using the analytical formula [24]

$$I = \frac{NZ_m\phi^{0.5}\sigma\tau_0\mu_m VA}{P^{1.5}L}\left[1-\exp\left(-\frac{L^2\phi^{0.5}P^{1.5}}{\tau_0\mu_m V}\right)\right], \tag{14}$$

where N [1/m^3] is the number density of the gas, proportional to its pressure P, V is the applied voltage, L the electrode spacing, μ_m the ion mobility inversely proportional to the mass m ($\mu_m \propto 1/m$) and the other symbols have the same meanings as in [24]. Moreover, the drift-diffusion model (6)-(7) can be solved analytically for the current density in the plate-parallel configuration [25]

$$J = \frac{e(\mu^+ + \mu^-)^2E^2}{2RL}\left[\sqrt{1+\frac{4RL^2S}{(\mu^+ + \mu^-)^2E^2}}-1\right], \tag{15}$$

where the ion-pair generation rate S is retrieved from the dose rate ϕ as [26]

$$S = \frac{\phi\rho}{eW}. \tag{16}$$

In (16) W is the energy for generating one ion-pair ($\approx$34 eV for SF_6) and ρ the gas density. The leakage

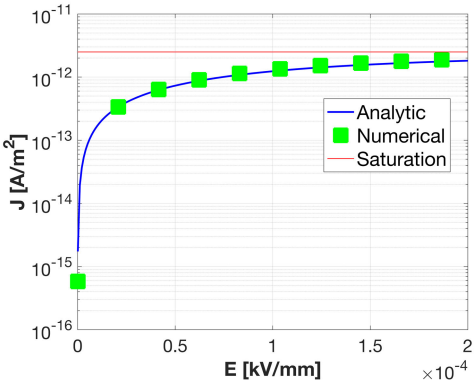

FIGURE 3. Curve of ionization region. The gap distance is L=50 cm and SF_6 @ 0.5 MPa is used as insulating gas. The equivalent current density calculated with (15) agrees with the analytical expression (15) and both tend towards the saturation value predicted by (17).

currents evaluated by the models are in good agreement and are reported in Fig. 3, which described the so-called ionization region exhibiting a saturation value controlled by the ion-pair generation rate [27],

$$J_{sat} = eSL. \tag{17}$$

In the saturation condition Eq. (14) reduces to [24]

$$I_{sat} = f_{gas}vP\phi, \tag{18}$$

where f_{gas} is a gas-dependent factor ($f_{gas} = 2.06$ for SF_6) and v the volume. Expression (18) can be conveniently use to estimate the power losses in the gas when the RIC effect takes place.

B. RELATIVE HUMIDITY INDUCED CONDUCTIVITY

The saturation condition predicted by (17)-(18), which is well reproduced by the transport model as described so far, is belied by experimental evidence for high electric stresses. As a matter of fact, as the electric field increases, an asymptotic value is not reached, but rather when $E \gtrsim 10-15$ kV/mm the current exhibits a rapid increase, which in principle could be attributed to Fowler-Nordheim (FN) or Schottky theories. However both of them fail to explain the experimental results.

Experimental evidence in SF_6 and fluoronitrile/CO_2 mixtures [28] says that the main parameters governing this phenomenon are the water content in the gas i.e., the relative humidity percentage (RH%) and the surface roughness of electrodes. Charged water particles lying on the thin layer of electrodes are injected due to local electric field enhancement, strictly related to the surface roughness [29]. In addition, the injection ratio seems to be slightly dependent on gas pressure. Referring to model (6)-(7), the injection phenomenon can be expressed as a Neumann condition on the cathode for the flux of negative ions $\mathbf{\Phi}_{n^-}$ [30]

$$-\mathbf{n}\cdot\mathbf{\Phi}_{n^-} = \frac{\sum_i j_i \exp(a_i E^{b_i})}{e}, \tag{19}$$

where $\mathbf{n}$ is the normal vector to the cathode and j_i, a_i, b_i are extrapolated from experimental observations. Generally the

injection phenomenon is referred to electrons, however due to the high electronegativity of the gas, no free electrons are considered in the model (6)-(7). These electrons attach themselves to neutral gas molecules thereby increasing the negative ions content. The injection region for high field stresses is shown in Fig. 4, by using the measured data from [31].

By appropriately tuning the ionization parameter S and the boundary conditions, the drift-diffusion model (6)-(7) can be used to determine the leakage current behaviour over a wide range of electric field stresses.

C. METAL PARTICLES

The contamination of metal particles produced during manufacturing and assembly stages may drastically reduce the dielectric capabilities of HVDC gas-insulated systems. Among the several trajectories followed by free conductive particle, two of them are particular dangerous [32]:

- The deposition of charged metal particle on solid insulator surfaces,
- The ''firefly'' phenomenon.

Metal particles attached to solid insulator may reduce the flashover voltage triggering to breakdown [33]. The ''firefly'' is a cyclic mechanism characteristic of HVDC gas-insulated systems operating in negative polarity; for example, this is the case of the AGPS gas-insulated components for N-NBIs. For a coaxial transmission line, the firefly can be described by looking at the motion of a positive charged particle towards the high voltage electrode. When the particle reaches the electrode it becomes negatively charged thus attracting a positive ion cloud. The particle tip enhances the electric field strength, which in turn reflects into emission of electrons and consequent formation of gas anions which move towards the outer conductor. If the electric force acting on the metal particle is sufficient to detach it, the positive ion cloud neutralize the particle and charge it positively restarting the process in a cyclic way [34]. To prevent the firefly phenomenon the so-called electrostatic traps has to be conceived, whose efficiency depend on the groove thickness and the trap width itself [35].

An empirical law to express the flux of injected negative ions due to local field enhancement driven by metal tips and/or rough surfaces is given by the micro-discharge flux formula [36]

$$-\mathbf{n}\cdot\mathbf{\Phi}_{n^-} = \tilde{k}\beta_{eff}E\left(\beta_{eff}E - \left(\frac{E}{P}\right)_0\right) \tag{20}$$

where $(E/P)_0$ is the critical reduced electric field for gas breakdown, β_{eff} is the field enhancement factor and $\tilde{k}$ [1/(V^2 ·s)] a correction coefficient.

IV. STREAMER BREAKDOWN INCEPTION

The prediction of the voltage holding capability of an HVDC gas-insulated components is of great interest from the engineering viewpoint. As a matter of fact, small metallic tips or inaccurate shape of the high voltage parts may enhance the electric field and even cause the electric breakdown of the gas-gap. As a precursor of the gas breakdown the streamer inception criterion can be exploited [37]

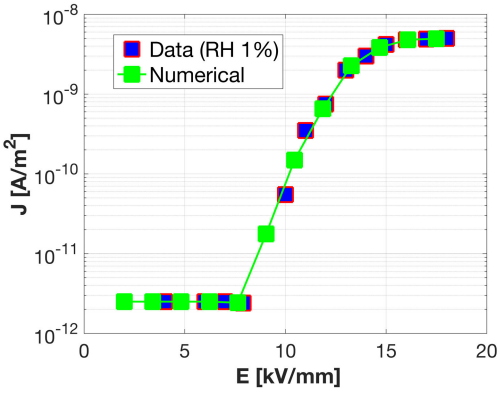

FIGURE 4. Curve of injection region at high electric fields for the plate-parallel geometry considering a relative humidity of 1%. Using (19), the numerical solution of (6) and (7) follows the experimental data.

$$\int_\Gamma \bar{\alpha}(E,P)ds = K \geq \ln(N_{cr}) = K_{cr}, \tag{21}$$

where N_{cr} is the critical number of electrons driving to avalanche and Γ the integration path tangent to the electric field lines. The integrand $\bar{\alpha}(E,P) := \alpha - \eta$ [1/m] is called effective ionization coefficient, difference between the first Townsend ionization coefficient α and the attachment coefficient η, function of electric field intensity and pressure. Usually, the reduced effective ionization $\bar{\alpha}/N = f(E/N)$ is used in literature, where N [1/m^3] is the number density of the gas related to P for example through the ideal gas law.

The increase in the number of electrons N_e along Γ is given by [38]

$$\frac{dN_e}{ds} = N_e\bar{\alpha}, \tag{22}$$

which predicts and exponential growth until $\alpha > \eta$. The critical reduced electric field $(E/N)_0$ correspond to the value for which $\bar{\alpha} = 0$. Once the trend of $\bar{\alpha}$ is known for the insulating gas adopted, for example from experimental fittings or by solving the collisional Boltzmann equation as stated in [14], the streamer criterion can be used in symbiosis with an optimization algorithm which allow to automatically redesign the critical parts of the geometry.

A. ALTERNATIVE INSULATING GASES

Sulphur hexafluoride because of its high dielectric strength, about 2.5 times higher than air, and its strong electronegativity, is widely used for electrical insulation systems since 1960, and represent the state-of-art gas for gas-insulated HVDC systems in nuclear fusion [39], [40], [41]. Due to its high GWP, SF_6 is listed in Kyoto protocol as greenhouse gas and alternative solutions are mandatory. The SF_6/N_2 mixtures (e.g., 20%/80%) represent a valid solution to reduce the amount of SF_6 while assuring high dielectric performances,

at the cost of increasing the operational pressure [42]. However, the environmental issue still caused by the presence of SF_6, pushed the research to more natural solutions, for example the N_2, O_2, CO_2 and N_2/O_2 mixtures. From experimental data [43] these mixtures reach dielectric performances comparable to SF_6/N_2 mixes, however, even in this case at the price of increasing the pressure level or the distance between anode and cathode parts with respect to pure SF_6 gas. Recently, novel fluorinated nitriles ($C_nF_{2n+1}CN$) for example the NOVEC^{TM} 4710 by 3M^{TM} company, trifluoroiodomethane (CF_3I) and fluoroketones ($C_nF_{2n}O$ for $n = 3, \ldots, 8$), might be candidate substitutes to pure SF_6 [44].

As stated above, one of the key parameters to estimate the dielectric performances of the insulating gas is the effective ionisation coefficient, required to verify the streamer condition (21) eventually used as a part of the shape optimization tool. A comparison of the trends of $\bar{\alpha}/N$ as a function of the reduced electric field E/N is shown in Fig. 5 for novel dielectric gases.

Looking at Table 3 it is clear that the novel solutions not only exhibits high dielectric performances, but are even more environmental friendly in view of their low GWP. These aspects are of great interest not only for the commercial HVDC gas-insulated systems but also for the development of the future equipments for nuclear fusion applications. In fact, in the early operational and manufacturing stages, the components must be frequently inspected thus requiring the storage of the gas in pressurized tanks. When using SF_6 the handling and storage units are critical components since no leaks into the atmosphere are allowed. Conversely, if natural gases are used e.g., N_2/O_2 mixtures, neither the evacuation system nor the storage units are critical, because the gas can be released freely in the atmosphere. However, as highlighted in [49] the novel gas solutions have some limitations that hinder their diffusion:

- High production costs,
- Higher operating pressure w.r.t. SF_6, thus requiring more stringent demands from the mechanical point of view,
- High boiling point (e.g. -4,7°C for the NOVEC^{TM} 4710 and -22.5°C for the CF_3I); because of this the gases need to be mixed with N_2 or CO_2 [50], [51],
- Compatibility with solid insulator materials and the effect of decomposition products [52].

For these reasons, hereinafter SF_6 is considered as baseline for the numerical analysis of HVDC gas-insulated systems in nuclear fusion field. However, the numerical methods here described can be equivalently used for the analysis of HVDC equipments using different gases, once the parameters to be used in the drift-diffusion model (6)-(7), e.g. the mobilities μ^+, μ^- or the equivalent conductivity σ_G for EQS model (1), are defined.

V. NUMERICAL RESULTS

The previous topics are numerically analyzed in this section using the commercial FEM software COMSOL® Multiphysics. Model (6)-(7) is realized in the Transport of Diluted Species (TDS) physics, while the electric field is evaluated by the Electric Currents module, assigning $\sigma_G = 0$ S/m to the gas and coupling the two analysis with a boundary current source given by the TDS [53]. The boundary and initial conditions for the model (6)-(7) are described in [14]. Specifically, the open boundary condition, available in TDS physics, is used for the ion densities n^+, n^-.

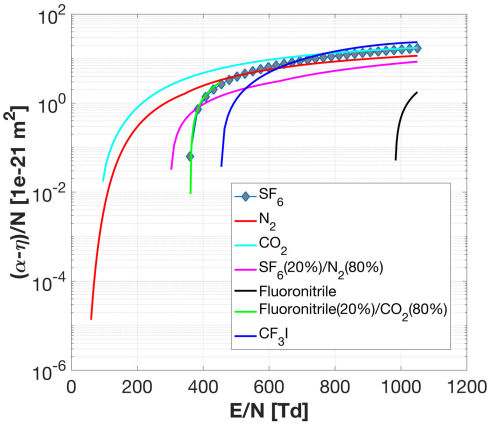

FIGURE 5. Reduced effective ionisation coefficient $\bar{\alpha}/N$ as a function of the reduced electric field E/N, for different insulating gases.

TABLE 3. Dielectric and environmental properties of insulating gases.

Gas	$(E/N)_0$ [Td]	GWP
SF_6	360 [45]	23900
N_2	60 [45]	0
CO_2	86 [45]	1
$N_2(60\%)/O_2(40\%)$	136.7 [46]	0.4
$SF_6(20\%)/N_2(80\%)$	260	4780
Fluoronitrile	981 [47]	2100
Fluoronitrile(20%)/CO_2(80%)	362.81 [47]	421
CF_3I	437 [44]	0.45 [49]

A. METAL PARTICLES INDUCED FIELD EMISSION

During its firefly motion the conducting metal particle may reach and attach to the high voltage electrode causing a local increase of the electric field intensity due to its small radii. In this example the leakage current emission and the possible streamer inception from the metallic tip are analyzed for a axisymmetric conical spacer retrieved from the numerical investigation of TL components of ITER NBI [13]. In the analysis, the solid insulator is characterized by $\sigma_I = 3.5 \cdot 10^{-15}$ S/m, $\sigma_S = 0$ S and $\varepsilon_r = 4$ and is embedded in a chamber with pressurized SF_6 at 0.5 MPa absolute with $\varepsilon_r = 1.002$. A voltage $U_{DC} = -550$ kV is applied to the high voltage electrode, where a small metal particle of radius 0.25 mm is attached.

Using (20) with $\beta_{eff} = 4$ and $\tilde{k} = 1.56 \cdot 10^{-3}$ 1/(V^2 ·s), the injection of negative ions from the metal tip can be included in the drift-diffusion model (6)-(7).

The enhanced leakage current caused by the negative ion emission due to the metal particle is highlighted in Fig. 6. Moreover, due to high field intensity in the tip

region, streamers can originate following Eq. 21. To consider the non-uniformity of the field, the critical electric field $(E/P)_0 = 85$ kV/(mm·MPa) of SF_6 is reduced by the field utilization factor $\xi = E_{avg}/E_{max} = 0.08$. The streamer integrals are shown in Fig. 6b from which a streamer inception channel satisfying $K \geq K_{cr} = 18.4$ is detected.

B. COUPLED ELECTRO-THERMAL ANALYSIS OF 2D TRANSMISSION LINE

In this example a 2D section of a transmission line is conceived. Referring to Fig. 7, the three acceleration voltages labelled HV_1, HV_2 and HV_3 are -510 kV, -334 kV and -167 kV respectively while the enclosure is referred to ground potential. The TL has an outer radius of 650 mm, that of HV_1 is 250 mm and the one of HV_2 and HV_3 is 50 mm. The -510 kV central conductor is supported by a solid post-insulator with conductivity expressed by (2) and $\varepsilon_r = 4.5$. SF_6 at 0.5 MPa absolute ($\rho = 39.7$ kg/m^3 at $T = 293.15$ K) is used as insulating gas.

In this example a comparison between the electrical model with and without the coupled thermal analysis described in section II-B is established. The electric current flowing in the central and intermediate conductors is $I_1 = 3150$ A, $I_2 = I_3 = 1$ A. I_1 was selected in accordance with literature values in the context of electro-thermal analysis of HVDC Gas Insulated Lines (GIL) [54]. The imposed voltages and currents have a square waveform of period $T = 3600$ s and duty-cycle $\delta = 0.28$. The TL is embedded in an air environment whose temperature at infinity is fixed at 293.15 K, while the surface emissivities of outer enclosure, inner enclosure, conductors and solid insulator are taken as $\epsilon = 0.92$, 0.93, 0.2 and 0.93 [19].

The electric field is evaluated with the EQS model (1) assigning the conductivity trends of (2) and (5) to solid and SF_6 gas domains respectively and the time integration lasts for $t = 28800$ s. The resulting electric field map for the coupled electro-thermal field problem is shown in Fig. 7 while the comparison of the trend of charge density accumulation $|\varrho_S|$, along the gas-solid interface is shown in Fig. 8. The difference is not that significant in the specific case, however the contribution of a precise modeling of thermal effects in charge accumulation is evident.

It is worth noting that in the specific case of the TL for the NBI of DTT the thermal effects are negligible, given the low value of the transmitted current (of the order of 50 A) and the short pulse duration. We wanted to quote this paragraph for the sake of completeness, as it is considered useful for a comprehensive description of the phenomena at play and the related modeling to take it into account.

C. 3D TRANSMISSION LINE OF DTT N-NBI

A 3D model of TL with the cross section defined in the previous example is here analyzed. The thermal analysis in this example is neglected due to the low temperature rise ΔT for the $t_{pulse} = 50$ s pulse length of DTT N-NBI with a current of $I = 60$ A in the central conductor. The temperature rise can be estimated under adiabatic conditions

$$\Delta T = \frac{P_R \times t_{pulse}}{m \times C_p} \text{ K}. \tag{23}$$

where P_R are the resistive power losses of the central conductor. Assuming the conductor made in Aluminium with conductivity of $\sigma_{alu} = 3.774 \cdot 10^7$ S/m, a thickness of 10 mm and a length of 1 meter, the resistive power losses are

$$P_R = RI^2 = 1.7 \cdot 10^{-6} \times 60^2 \approx 6.2 \cdot 10^{-3} \text{ W}. \tag{24}$$

The SF_6 mass is approximately of $m \approx 43$ kg, thus from (23) $\Delta T = 1.1 \cdot 10^{-5}$ K. The gas temperature is fixed to $T = 293.15$ K.

A comparison between the transient behavior of drift-diffusion (6)-(7) and EQS (1) is established using the electric conductivity of SF_6 given by (5) in the latter. A slice of the electric field map after $t = 50$ s from the solution of the drift-diffusion model is reported in Fig. 9 while a comparison between the electric field components along the creepage length of the solid insulator calculated by the two approaches is shown in Fig. 10.

Under ideal condition i.e. without considering charge injection, the two results are very similar, however things can substantially change when localized injection phenomena occur, for example due to a small metallic tip.

D. SF_6-AIR BUSHING OF DTT N-NBI

The electric distribution system of DTT N-NBI foresees two SF_6-air bushings: one is located in a closed building and connects the TL with the high voltage deck (HVD); the other is used for the electrical connection between the last part of the TL and the NBI inside the Tokamak hall [7]. The latter is characterized by three feedthrough each of −510 kV, −334 kV and −167 kV, supplying the acceleration grids. In this example the attention is focused on the design of the −510 kV bushing for the HVD. The HVD is a Faraday cage made of $AlMg_3$ panels insulated from ground for -510 kV, housing the ISEPS acronym for Ion Source and Extraction Power Supply. Its external dimensions of 16 m (L) × 9 m (W) × 5 m (H) are scaled from that of the 100 kV HVD of SPIDER experiment in PRIMA test facility [55]. The 3D CAD of the buildings including the HVD and the bushing is given in Fig. 11. The high voltage components installed in closed buildings have to comply environmental constraints as given in Table 4 [56]. Following the design roadmap of the HVD for the ITER NBI, the 1 kV/mm electric field limit in air accounts for a safety margin of factor three with respect to the theoretical breakdown strength of dry air (≈ 3 kV/mm) [57]. To this aim, an electrostatic analysis is carried out for a simplified 3D model which neglects the HVD insulators and small geometrical features of the bushing (for example the silicone rubber sheds). Results are shown in Fig. 12 for a X-Z cut plane. As expected, the intensity of electric field is higher inside the bushing, however the limit of 1 kV/mm in

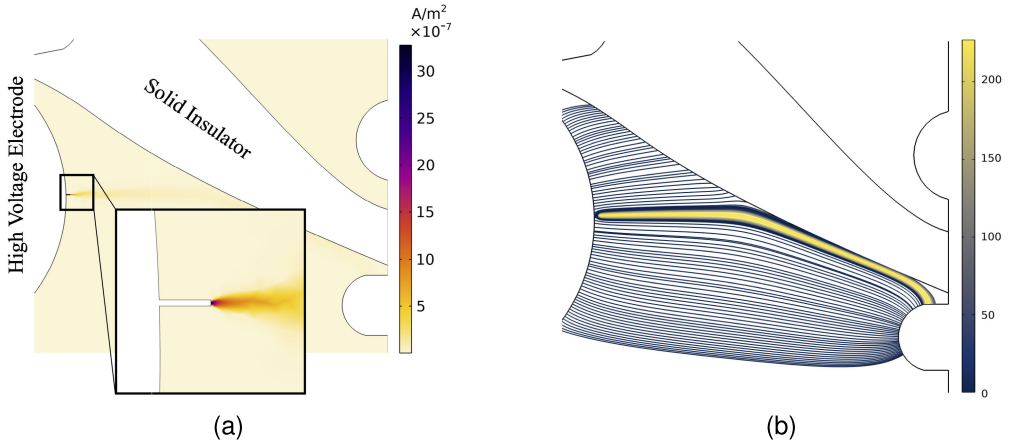

FIGURE 6. Effect of small metallic defect. (a) Leakage current enhancement. (b) Streamer inception. The color-bar refers to values of the streamer integrals via (21).

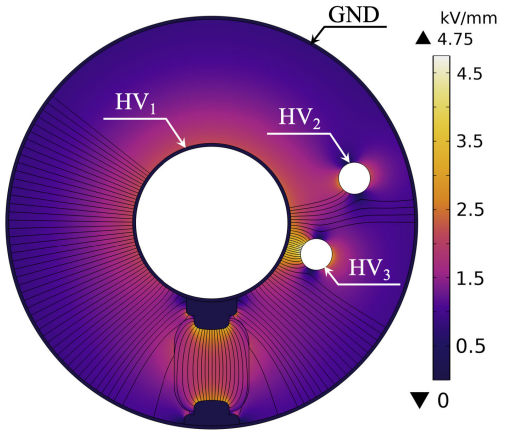

FIGURE 7. Voltage labels and electric field intensity after $t = 25500$ s of time simulation.

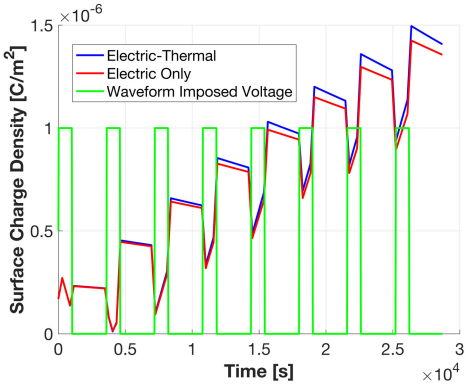

FIGURE 8. Normalized waveform of imposed currents and voltages (green) together with the absolute value of surface charge density accumulation trend in coupled electric-thermal (blue) and electric only analysis (red). The time integration runs for $t = 28800$ s after which no steady station condition is reached.

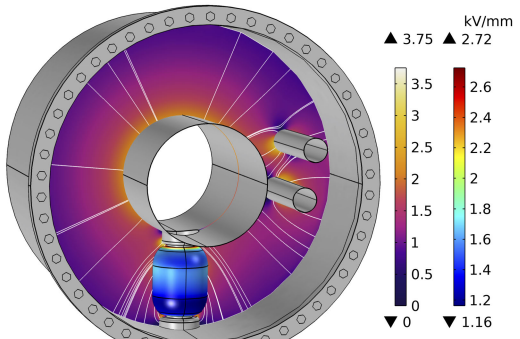

FIGURE 9. Electric field intensity of TL evaluated with the time-dependent drift-diffusion model (6)-(7) after $t = 50$ s simulation.

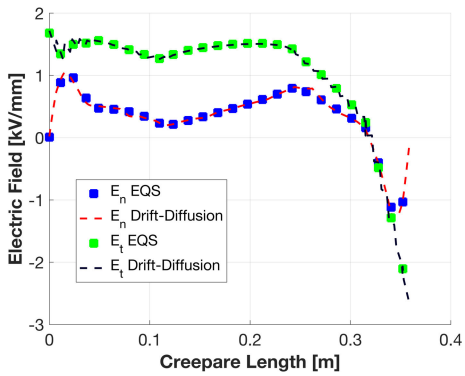

FIGURE 10. Normal (E_n) and tangential (E_t) electric field components along the creepage length of the post insulator after $t = 50$ s, evaluated with drift-diffusion and EQS models.

air is never exceeded. The conceptual design of the bushing requires particular effort to avoid possible breakdown channels, both in SF_6 and air. In fact, a realistic model of the bushing must include small geometrical features, like the sheds, where the electric field intensity can be enhanced. The possibility of adopting a FGM material to homogenize the electric field along the bushing sheds is investigated using a 2D axisymmetric model. The bushing sheds are made of silicone rubber with $\sigma_{SiR} = 5 \cdot 10^{-16}$ S/m and $\varepsilon_r = 2.8$, while for the epoxy parts $\sigma_I = 1.6 \cdot 10^{-16}$ S/m and $\varepsilon_r = 4.5$. A thin layer of 5 mm of FGM is placed within the silicone rubber domain next to the grounded electrode of the bushing. For such material the electrical conductivity (4) is used with

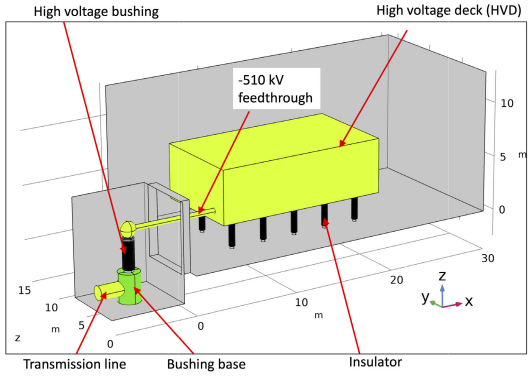

FIGURE 11. Draft 3D CAD of HVD and bushing buildings for the AGPS of DTT NBI.

TABLE 4. Environmental parameters inside HVD and bushing buildings.

Parameter	Value
Temperature (min ÷ max)	18°C ÷ 35°C
Air humidity (min ÷ max)	40% ÷ 60%
Dust class	100.000 P/ft^3
Max. electric field strength in air	1 kV/mm

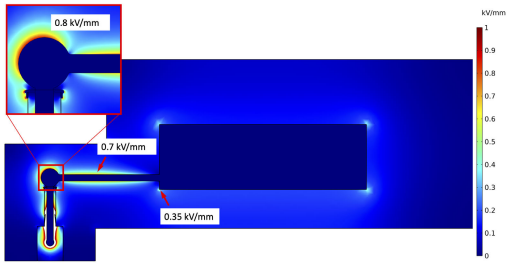

FIGURE 12. Electric field intensity on a X-Z cut plane of the HVD and bushing buildings. The electric field strength inside the bushing exceeds 1 kV/mm.

$\sigma_{I0} = 10^{-3}$ S/m, $E_1 = 0.7$ kV/mm, $E_2 = 2.23$ kV/mm, $\gamma = 8$ and $\varepsilon_r = 12$. As illustrated in Fig. 13 the peak of electric field intensity in air along the sheds, after $t = 50$ s of EQS analysis, is reduced below 1 kV/mm.

From the previous considerations a 3D bushing model for the HVD is conceived and is given in Fig. 14. The model includes also a section of the TL connected to the bushing base, whose central conductor is supported by a conical solid insulator and the grounded walls of the building. The FEM solution requires particular attention in the discretization phase of the domain (mesh) due to the very different scales of the geometric features.

The electric field map of the whole component on a Y-Z cut plane is shown in Fig. 15 at time $t = 50$ s.

The bushing located inside the Tokamak hall is subjected to a radiation field coming from the fusion machine, thus the RIC effect has to be considered. An estimation of the power losses is mandatory to understand the need of radiation screens or insulating techniques different from pressurized SF_6. Assuming a dose rate $\phi = 2.6$ mGy/s [58] and a volume $v \approx 4$ m^3 of SF_6, formula (18) gives $I_{sat} \approx 10$ mA, which for a polarization of 510 kV results in $P_{loss,RIC} \approx 5.5$ kW.

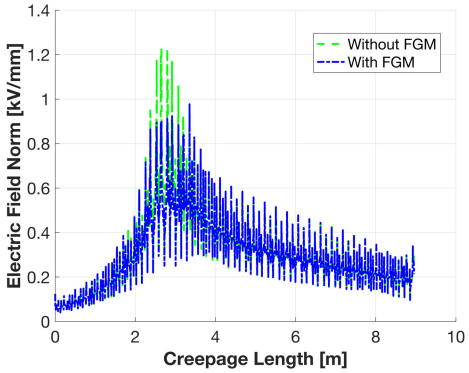

FIGURE 13. Electric field norm along bushing sheds in air after $t = 50$ s of EQS analysis. Using the FGM the peak value is reduced of about 20%. The creepage length is measured from the bottom to top of the bushing.

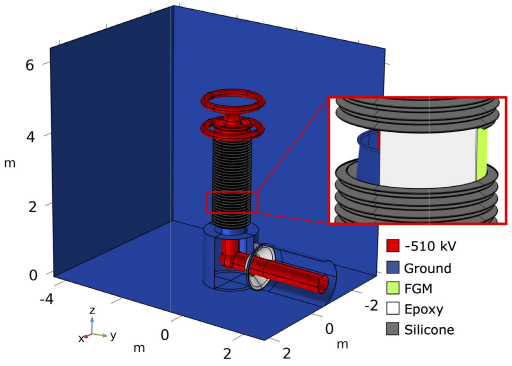

FIGURE 14. Cutaway of the 3D CAD of the bushing for TL2-HVD connection. The inset shows the inner material in the position of the grounded electrode where the FGM layer is located.

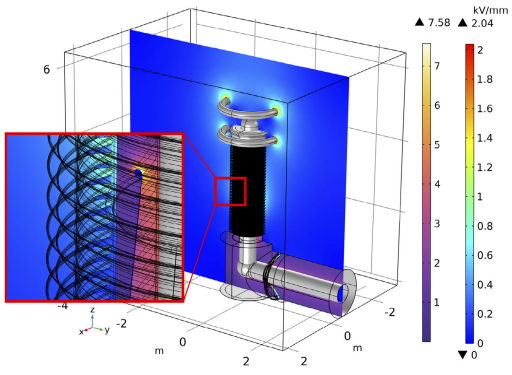

FIGURE 15. Electric field map on Y-Z cut plane. The inset shows the electric field intensity next to the grounded ring electrode where the FGM layer is placed.

These power losses seems to be acceptable also considering the short duration of the DTT NBI pulses, therefore no further actions are currently planned.

VI. CONCLUSION

In this paper the numerical techniques used to analyze the electric field distribution of HVDC gas-insulated components for the AGPS of DTT N-NBI were described. Particular emphasis was given in the leakage current modeling driven by external ionization fields and due to the field emission caused

by the random firefly motion of metallic particles attached to the high voltage conductor. The leakage current induced by the residual water content in the gas (%RH) and the surface roughness can drastically reduce the dielectric capabilities of the system and must be considered during the operational phase.

Although SF_6 is the most common gas, its high GWP limit its usage for the future HVDC gas-insulated systems, therefore alternative solutions with less environmental impact were therein considered, mainly with the purpose of establishing the trend of the effective ionization coefficient required for the streamer inception analysis. The novel gases generally require mixing with other species and increasing operational pressure levels, which impact to the mechanical design of the components. The applicability of such gases for the development of future HVDC equipments for nuclear fusion will be of interest in future investigations.

The EQS and drift-diffusion models were applied for the preliminary investigation of the multi-conductor TL used to carry the power from the AGPS generators to the N-NBI inside the Tokamak hall and for the design of the SF_6-air bushing feeding the HVD. As far as no field emission occur, for example due to small metallic tips, the EQS model can be conveniently applied, however to account for the local behaviour of charge carriers the drift-diffusion model is mandatory. The road map to the final design of the components, in particular for the SF_6-air bushing to be placed in the Tokamak hall, requires further improvements of the discussed configuration, in particular the inclusion of the feedthrough of intermediate acceleration voltages.

REFERENCES

[1] T. Inoue, M. Kashiwagi, M. Taniguchi, M. Dairaku, M. Hanada, K. Watanabe, and K. Sakamoto, "1 MeV, ampere class accelerator R&D for ITER," *Nucl. Fusion*, vol. 46, no. 6, pp. S379–S385, Jun. 2006.

[2] V. Toigo, R. Piovan, S. D. Bello, E. Gaio, A. Luchetta, R. Pasqualotto, P. Zaccaria, M. Bigi, G. Chitarin, and D. Marcuzzi, and N. Pomaro, "The prima test facility: Spider and MITICA test-beds for iter neutral beam injectors," *New J. Phys.*, vol. 19, no. 8, 2017, Art. no. 085004.

[3] R. Martone, R. Albanese, F. Crisanti, A. Pizzuto, and M. Piero, *DTT—Divertor Tokamak Test Facility—Interim Design Report*. Stockholm, Sweden: ENEA, Apr. 2019.

[4] R. Ambrosino, "DTT—Divertor tokamak test facility: A testbed for DEMO," *Fusion Eng. Des.*, vol. 167, Jun. 2021, Art. no. 112330.

[5] Y. Ikeda, N. Akino, N. Ebisawa, M. Hanada, T. Inoue, A. Honda, M. Kamada, M. Kawai, M. Kazawa, and K. Kikuchi, "Technical design of NBI system for JT-60 SA," *Fusion Eng. Design*, vol. 82, nos. 5–14, pp. 791–797, Oct. 2007.

[6] P. Agostinetti, E. Benedetti, T. Bolzonella, M. Bonesso, I. Casiraghi, R. Dima, G. Favero, A. Ferro, M. Gobbin, G. Granucci, and C. Hu, "Conceptual design of the beamline for the DTT neutral beam injector following a double beam source design approach," *Plasma Fusion Res.*, vol. 16, Jun. 2021, Art. no. 2405080.

[7] A. Ferro, F. Lucchini, P. Agostinetti, D. Ratti, G. Granucci, A. Romano, R. Romano, A. Cucchiaro, and A. Princiotta, "Conceptual design of the power supplies for DTT neutral beam injector," *Fusion Eng. Des.*, vol. 169, Aug. 2021, Art. no. 112624.

[8] P. Agostinetti, E. Benedetti, R. Bonifetto, M. Bonesso, M. Cavenago, S. D. Bello, M. D. Palma, D. D'Ambrosio, R. Dima, G. Favero, and A. Ferro, "Improved conceptual design of the beamline for the DTT neutral beam injector," *IEEE Trans. Plasma Sci.*, vol. 50, no. 11, pp. 4027–4032, Nov. 2022.

[9] R. Torchio, V. Cirimele, P. Alotto, and F. Freschi, "Modelling of road–embedded transmitting coils for wireless power transfer," *Comput. Electr. Eng.*, vol. 88, Dec. 2020, Art. no. 106850.

[10] P. Bettini, R. Specogna, and F. Trevisan, "Electroquasistatic analysis of the gas insulated line for the ITER neutral beam injector," *IEEE Trans. Magn.*, vol. 45, no. 3, pp. 996–999, Mar. 2009.

[11] N. Zebouchi, H. Li, and M. A. Haddad, "Development of future compact and eco-friendly HVDC gas-insulated systems: Shape optimization of a DC spacer model and novel materials investigation," *Energies*, vol. 13, no. 12, p. 3288, Jun. 2020.

[12] E. Volpov, "Electric field modeling and field formation mechanism in HVDC SF_6 gas insulated systems," *IEEE Trans. Dielectr. Electr. Insul.*, vol. 10, no. 2, pp. 204–215, Apr. 2003.

[13] A. D. Lorenzi, L. Grando, A. Pesce, P. Bettini, and R. Specogna, "Modeling of epoxy resin spacers for the 1 MV DC gas insulated line of ITER neutral beam injector system," *IEEE Trans. Dielectr. Electr. Insul.*, vol. 16, no. 1, pp. 77–87, Feb. 2009.

[14] F. Lucchini, N. Marconato, and P. Bettini, "Automatic optimization of gas insulated components based on the streamer inception criterion," *Electronics*, vol. 10, no. 18, p. 2280, Sep. 2021.

[15] J. Li, H. C. Liang, B. X. Du, and Z. H. Wang, "Surface functional graded spacer for compact HVDC gaseous insulated system," *IEEE Trans. Dielectr. Electr. Insul.*, vol. 26, no. 2, pp. 664–667, Apr. 2019.

[16] H. Ye, M. Clemens, J. Schulte-Fischedick, and J. Seifert, "Investigation of electrical field grading of bushings with microvaristor filled epoxy resin components," in *Proc. IEEE Int. Power Modulator High Voltage Conf. (IPMHVC)*, Jun. 2014, pp. 153–156.

[17] C. Jörgens, H. Hensel, and M. Clemens, "Modeling of the electric field in high voltage direct current gas insulated transmission lines," in *Proc. IEEE 4th Int. Conf. Dielectr. (ICD)*, Jul. 2022, pp. 134–137.

[18] R. Morrow, "A survey of the electron and ion transport properties of SF_6," *IEEE Trans. Plasma Sci.*, vol. PS-14, no. 3, pp. 234–239, Jun. 1986.

[19] X. Li, M. Wan, S. Yan, and X. Lin, "Temperature and electric field distribution characteristics of a DC-GIL basin-type spacer with 3D modelling and simulation," *Energies*, vol. 14, no. 23, p. 7889, Nov. 2021.

[20] Y. Fujiwara, T. Inoue, K. Miyamoto, N. Miyamoto, Y. Ohara, Y. Okumura, and K. Watanabe, "Influence of radiation on insulation gas at the ITER–NBI system," *Fusion Eng. Des.*, vol. 55, no. 1, pp. 1–8, May 2001.

[21] N. Pilan, P. Bettini, A. De Lorenzi, and R. Specogna, "Voltage holding optimization of the MITICA electrostatic accelerator," *Fusion Eng. Des.*, vol. 88, nos. 6–8, pp. 1038–1041, Oct. 2013.

[22] G. Chitarin, A. Kojima, M. Boldrin, A. Luchetta, D. Marcuzzi, P. Zaccaria, L. Zanotto, V. Toigo, D. Aprile, N. Marconato, and T. Patton, "Strategy for vacuum insulation tests of MITICA 1 MV electrostatic accelerator," *IEEE Trans. Plasma Sci.*, vol. 50, no. 9, pp. 2755–2762, Sep. 2022.

[23] L. Zanotto, A. Maistrello, M. Boldrin, M. Bigi, R. Casagrande, M. De Nardi, E. Gaio, D. Marcuzzi, M. Recchia, V. Toigo, C. Rotti, H. Decamps, P. Veltri, J. Zacks, D. Gutierrez, and M. Simon, "Radio frequency generators based on solid state amplifiers for the NBTF and ITER projects," *IEEE Trans. Plasma Sci.*, vol. 50, no. 11, pp. 3970–3976, Nov. 2022.

[24] E. R. Hodgson and A. Moroño, "A model for radiation induced conductivity in neutral beam injector insulator gases," *J. Nucl. Mater.*, vols. 307–311, pp. 1660–1663, Dec. 2002. [Online]. Available: https://www.sciencedirect.com/science/article/pii/S0022311502012989

[25] J. Kindersberger and C. Lederle, "Surface charge decay on insulators in air and sulfurhexafluorid—Part I: Simulation," *IEEE Trans. Dielectr. Electr. Insul.*, vol. 15, no. 4, pp. 941–948, Aug. 2008.

[26] I. Lopes, H. Hilmert, and W. F. Schmidt, "Ionisation of gaseous and liquid sulphur hexafluoride by ^{60}Co γ-radiation," *J. Phys. D, Appl. Phys.*, vol. 19, no. 6, pp. L107–L110, Jun. 1986.

[27] W. F. Schmidt, "Radiation-induced conductivity and ion yields in neopentane at high electric fields," *Radiat. Res.*, vol. 42, no. 1, pp. 73–78, Apr. 1970.

[28] C. Toigo, T. Vu-Cong, F. Jacquier, and A. Girodet, "DC leakage current measurement comparison between SF_6 and Fluoronitrile/CO_2 gas mixture," in *Proc. IEEE 3rd Int. Conf. Dielectr. (ICD)*, Jul. 2020, pp. 790–793.

[29] L. Zavattoni, R. Hanna, O. Lesaint, and O. Gallot-Lavallée, "Dark current measurements in humid SF_6: Influence of electrode roughness, relative humidity and pressure," *J. Phys. D, Appl. Phys.*, vol. 48, no. 37, Sep. 2015, Art. no. 375501.

[30] L. Zavattoni, C.-T. Vu, P. Vinson, and A. Girodet, "Leakage current measurements in direct current gas insulated substations equipment," in *Proc. IEEE Int. Conf. Dielectr. (ICD)*, vol. 2, Jul. 2016, pp. 860–863.

[31] R. Hanna, O. Lesaint, and L. Zavattoni, "Dark current measurements in humid SF_6 at high uniform electric field," in *Proc. IEEE Conf. Electr. Insul. Dielectr. Phenomena (CEIDP)*, Oct. 2016, pp. 19–22.

[32] J. Wang, Q. Hu, Y. Chang, J. Wang, R. Liang, Y. Tu, C. Li, and Q. Li, "Metal particle contamination in gas-insulated switchgears/gas-insulated transmission lines," *CSEE J. Power Energy Syst.*, vol. 7, no. 5, pp. 1011–1025, 2019.

[33] X. Li, C. Cao, and X. Lin, "Influence of conducting particle on DC flashover characteristics and tracking property of GIS/GIL insulator," *IEEE Access*, vol. 10, pp. 17212–17220, 2022.

[34] A. Diessner and J. Trump, "Free conducting particles in a coaxial compressed-gas-insulated system," *IEEE Trans. Power App. Syst.*, vol. PAS-89, no. 8, pp. 1970–1978, Nov. 1970.

[35] W. Zhiyuan, W. Jian, L. Qingmin, N. Xiaoru, and L. Botao, "Three dimensional simulating and experimental study on the influential factors of the effectiveness of the DC-GIL particle trap," in *Proc. 1st Int. Conf. Electr. Mater. Power Equip. (ICEMPE)*, May 2017, pp. 544–547.

[36] H. C. Liang, B. X. Du, and J. Li, "Electric field regulation and parameter optimization of surface nonlinear conductivity spacer for 500 kV DC-GIL," *IEEE Trans. Dielectr. Electr. Insul.*, vol. 27, no. 4, pp. 1330–1338, Aug. 2020.

[37] N. Malik, "Streamer breakdown criterion for compressed gases," *IEEE Trans. Electr. Insul.*, vol. EI-16, no. 5, pp. 463–467, Oct. 1981.

[38] N. Malik and A. Qureshi, "Breakdown mechanisms in sulphur-hexafluoride," *IEEE Trans. Electr. Insul.*, vol. EI-13, no. 3, pp. 135–145, Jun. 1978.

[39] H. Tobari, K. Watanabe, M. Kashiwagi, H. Yamanaka, T. Maejima, Y. Terunuma, A. Kojima, M. Dairaku, and M. Hanada, "DC ultrahigh voltage insulation technology for 1 MV power supply system for fusion application," *IEEE Trans. Plasma Sci.*, vol. 45, no. 1, pp. 162–169, Jan. 2016.

[40] A. Takahashi, T. Suto, H. Fujita, Y. Hiranuma, S. Ichimura, K. Watanabe, M. Kashiwagi, H. Tobari, and T. Maejima, "–1 MV DC filter and high-voltage DC measurement system for ITER neutral beam injector system," *IEEE Trans. Power Electron.*, vol. 36, no. 7, pp. 7587–7599, Jul. 2020.

[41] A. Takahashi, T. Suto, T. Tanaka, K. Yamaguchi, H. Fujita, Y. Hiranuma, S. Ichimura, K. Watanabe, M. Kashiwagi, T. Maejima, and H. Tobari, "1 MV rectifier with SF_6-gas insulation and cooling for ITER neutral beam injector system," *IEEE Trans. Ind. Appl.*, vol. 57, no. 5, pp. 4398–4408, Sep. 2021.

[42] L. G. Christophorou and R. J. Van Brunt, "SF_6/N_2/mixtures: Basic and HV insulation properties," *IEEE Trans. Dielectr. Electr. Insul.*, vol. 2, no. 5, pp. 952–1003, Oct. 1995.

[43] T. Rokunohe, Y. Yagihashi, F. Endo, and T. Oomori, "Fundamental insulation characteristics of air; N_2, CO_2, N_2/O_2, and SF_6/N_2 mixed gases," *Electr. Eng. Jpn.*, vol. 155, no. 3, pp. 9–17, 2006.

[44] A. Beroual and A. M. Haddad, "Recent advances in the quest for a new insulation gas with a low impact on the environment to replace sulfur hexafluoride (SF_6) gas in high-voltage power network applications," *Energies*, vol. 10, no. 8, p. 1216, Aug. 2017.

[45] T. Liu, I. V. Timoshkin, S. J. MacGregor, M. P. Wilson, M. J. Given, N. Bonifaci, and R. Hanna, "Field-time breakdown characteristics of air, N_2, CO_2, and SF_6," *IEEE Trans. Plasma Sci.*, vol. 48, no. 10, pp. 3321–3331, Oct. 2020.

[46] H. Zhao and H. Lin, "Dielectric breakdown properties of N_2–O_2 mixtures by considering electron detachments from negative ions," *Phys. Plasmas*, vol. 23, no. 7, Jul. 2016, Art. no. 073505.

[47] H. E. Nechmi, A. Beroual, A. Girodet, and P. Vinson, "Effective ionization coefficients and limiting field strength of fluoronitriles-CO_2 mixtures," *IEEE Trans. Dielectr. Electr. Insul.*, vol. 24, no. 2, pp. 886–892, Apr. 2017.

[48] X. Li, H. Zhao, J. Wu, and S. Jia, "Analysis of the insulation characteristics of CF_3I mixtures with CF_4, CO_2, N_2, O_2 and air," *J. Phys. D, Appl. Phys.*, vol. 46, no. 34, 2013, Art. no. 345203.

[49] G. Chen, Y. Tu, C. Wang, J. Wang, Z. Yuan, G. Ma, J. Wang, B. Qi, and C. Li, "Environment-friendly insulating gases for HVDC gas-insulated transmission lines," *CSEE J. Power Energy Syst.*, vol. 7, no. 3, pp. 510–529, 2019.

[50] H. E. Nechmi, A. Beroual, A. Girodet, and P. Vinson, "Fluoronitriles/CO_2 gas mixture as promising substitute to SF_6 for insulation in high voltage applications," *IEEE Trans. Dielectr. Electr. Insul.*, vol. 23, no. 5, pp. 2587–2593, Oct. 2016.

[51] L. Chen, P. Widger, M. S. Kamarudin, H. Griffiths, and A. Haddad, "CF_3I gas mixtures: Breakdown characteristics and potential for electrical insulation," *IEEE Trans. Power Del.*, vol. 32, no. 2, pp. 1089–1097, Apr. 2017.

[52] W. Gao, Y. Cao, Y. Wang, C. Price, J. Ronzello, N. Uzelac, A. Laso, M. Tefferi, and K. Darko, "Materials compatibility study of C_4F_7N/CO_2 gas mixture for medium-voltage switchgear," *IEEE Trans. Dielectr. Electr. Insul.*, vol. 29, no. 1, pp. 270–278, Feb. 2022.

[53] N. Lavesson and C. Doiron, "Hybrid resistive-capacitive and ion drift model for solid gas dielectrics," in *Proc. COMSOL Conf.*, 2015, pp. 1–6.

[54] X. Li, S. Han, M. Wan, W. Wang, Z. Geng, and X. Lin, "Transient surface charge characteristics of DC-GIL insulator under thermal-electric coupled fields," *IEEE Access*, vol. 10, pp. 19447–19457, 2022.

[55] M. Boldrin, L. Grando, A. Pesce, M. Recchia, V. Toigo, D. Gutierrez, M. Simon, G. Faoro, A. Guion, E. Maggiora, D. Pedron, A. Roman, and H. Decamps, "The 100 kV Faraday cage (high voltage deck) for the SPIDER experiment," *Fusion Eng. Des.*, vols. 96–97, pp. 411–415, Oct. 2015.

[56] M. Boldrin, M. Simon, G. E. Gomez, M. Krohn, H. Decamps, T. Bonicelli, and V. Toigo, "The high voltage deck 1 and bushing for the ITER neutral beam injector: Integrated design and installation in MITICA experiment," *Fusion Eng. Des.*, vol. 146, pp. 1895–1898, Sep. 2019.

[57] M. Boldrin, A. De Lorenzi, H. Decamps, L. Grando, M. Simon, and V. Toigo, "Design status and procurement activities of the high voltage deck 1 and bushing for the ITER neutral beam injector," *Fusion Eng. Des.*, vol. 88, nos. 6–8, pp. 985–989, Oct. 2013.

[58] A. Colangeli, R. Villari, R. Luis, F. Moro, S. Sandri, N. Fonnesu, D. Flammini, G. Mariano, F. Crisanti, G. Ramogida, and F. Lucca, "Neutronics study for DTT tokamak building," *Fusion Eng. Des.*, vol. 146, pp. 2581–2585, Sep. 2019.

FRANCESCO LUCCHINI received the M.S. degree in mathematical engineering from the University of Padua, Padua, Italy, in 2019. He is currently pursuing the joint Ph.D. degree in fusion science and engineering with the University of Padua and the University of Ghent, Ghent, Belgium. His research interests include numerical methods, optimizations, and modeling of gas insulated high voltage components for neutral beam injectors.

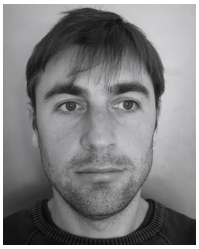

NICOLÒ MARCONATO (Member, IEEE) is currently an Assistant Professor of electrical engineering with the Department of Industrial Engineering, University of Padua. He is mainly involved in numerical and applied electromagnetism, particularly in the field of fusion research and high-energy physics and engineering. He has also applied and developed codes for the numerical solution of electromagnetic propagation, electromagnetic compatibility (EMC), coupled problems (multiphysics), optimization problems, and MV/HV gas and vacuum insulated components. His research activities are based on an extensive network of international collaborations between research groups working at major universities and public and private research centers in Europe and beyond, as evidenced by numerous joint scientific papers listed in international databases (Scopus and Web of Science). He has published about 100 papers in international journals and contributions to international conferences (H-index: 20).

Open Access funding provided by 'Università degli Studi di Padova' within the CRUI CARE Agreement